doi:10.1016/j.jmb.2010.10.048 J. Mol. Biol. (2011) 405, 227–237

Contents lists available at www.sciencedirect.com

Journal of Molecular Biology

journal homepage: http://ees.elsevier.com.jmb

First Structures of an Active Bacterial Tyrosinase Reveal Copper Plasticity

Mor Sendovski[1]†, Margarita Kanteev[2]†, Vered Shuster Ben-Yosef[1], Noam Adir[2] and Ayelet Fishman[1]*

[1]*Department of Biotechnology and Food Engineering, Technion—Israel Institute of Technology, Haifa 32000, Israel*
[2]*Schulich Department of Chemistry, Technion—Israel Institute of Technology, Haifa 32000, Israel*

Received 21 August 2010; received in revised form 23 October 2010; accepted 26 October 2010
Available online 30 October 2010

Edited by R. Huber

Keywords:
tyrosinase;
crystal structure;
copper;
Bacillus megaterium

Tyrosinase is a member of the type 3 copper enzyme family that is involved in the production of melanin in a wide range of organisms. The crystal structures of a tyrosinase from *Bacillus megaterium* were determined at a resolution of 2.0–2.3 Å. The enzyme crystallized as a dimer in the asymmetric unit and was shown to be active in crystal. The overall monomeric structure is similar to that of the monomer of the previously determined tyrosinase from *Streptomyces castaneoglobisporus*, but it does not contain an accessory Cu-binding "caddie" protein. Two Cu(II) ions, serving as the major cofactors within the active site, are coordinated by six conserved histidine residues. However, determination of structures under different conditions shows varying occupancies and positions of the copper ions. This apparent mobility in copper binding modes indicates that there is a pathway by which copper is accumulated or lost by the enzyme. Additionally, we suggest that residues R209 and V218, situated in a second shell of residues surrounding the active site, play a role in substrate binding orientation based on their flexibility and position. The determination of a structure with the inhibitor kojic acid, the first tyrosinase structure with a bound ligand, revealed additional residues involved in the positioning of substrates in the active site. Comparison of wild-type structures with the structure of the site-specific variant R209H, which possesses a higher monophenolase/diphenolase activity ratio, lends further support to a previously suggested mechanism by which monophenolic substrates dock mainly to CuA.

Introduction

Tyrosinase (EC 1.14.18.1) is a type 3 copper enzyme that performs two successive reactions in the presence of molecular oxygen: hydroxylation of phenols to form *ortho*-diphenols (monophenolase activity) and oxidation of *o*-diphenols to *o*-quinones (diphenolase activity).[1,2] The reactive quinones polymerize spontaneously to form melanin, which is the source of skin pigmentation and fruit/vegetable browning. Tyrosinase is abundant in mammals, plants, fungi, and bacteria, and the active site is well conserved among the different species.[3–7] Six histidine residues, which are provided by a four-helical bundle, coordinate the two copper ions (CuA and CuB) in the active site.[1,8]

Three different states of the active site have been reported: the oxygenated oxy form (E_{ox}; [Cu^{II}–O_2^{2-}–Cu^{II}]), the oxidized Cu(II)-containing met form (E_m;

*Corresponding author. E-mail address: afishman@tx.technion.ac.il.

† M.S. and M.K. contributed equally to this article.

Abbreviations used: TyrSc, tyrosinase from *Streptomyces castaneoglobisporus*; TyrBm, tyrosinase from *Bacillus megaterium*; PDB, Protein Data Bank; L-DOPA, L-dihydroxyphenylalanine.

0022-2836/$ - see front matter

[Cu^{II}–Cu^{II}]), and the reduced deoxy form (E_d; [Cu^{I}–Cu^{I}]).[5,9] E_{ox} is able to catalyze the hydroxylation of monophenolic substrates and the oxidation of diphenols, whereas E_m results in a dead-end complex with monophenols and cannot bind oxygen.[10] In the oxy form, molecular oxygen is proposed to be bound as a peroxide between the two copper atoms in a side-on conformation, as visualized in previously determined crystal structures.[11] In the absence of any substrate, E_m is the primary form.[10]

Two other members of the type 3 copper protein family are catechol oxidases (EC 1.10.3.1), which only perform diphenolase activity, and hemocyanins, which are oxygen carriers from the hemolymph of many molluscs and arthropods.[12–14] Although the active centers of the type 3 copper proteins are similar in their overall structure and their ability to bind molecular oxygen, their potential enzymatic activities are different, suggesting a large variation in the substrate-binding pocket or in the accessibility of the substrate to the active site.[1,11] To date, there are two crystal structures of catechol oxidase,[14,15] three crystal structures of hemocyanin,[16–18] one crystal structure of an arthropod prophenoloxidase,[19] and one crystal structure of a tyrosinase from *Streptomyces castaneoglobisporus* (TyrSc) crystallized in complex with a caddie protein.[11] The caddie protein, expressed from *orf378*, is necessary for obtaining a functional form of the bacterial enzyme and is believed to perform a chaperone-like function in providing the copper ions to the tyrosinase.[11] However, the enzyme is inactive while in complex with the caddie protein. From structure–function investigations, it appears that access to the active site in hemocyanins is blocked, and the only physiological role that remains is the binding and transport of O_2.[18,20,21] In contrast, the active sites of tyrosinases and catechol oxidases are near the protein surface, allowing substrates to more easily access the dicopper center. Although the CuB site is strictly conserved for tyrosinases and catechol oxidases, the CuA environment has more variations and seems to tune the proteins to perform their specific activities.[22] Due to the complexity of the enzymatic mechanism of tyrosinase, the precise interactions and residues responsible for substrate orientation have been difficult to assign definitively.

We have recently isolated and characterized a tyrosinase from *Bacillus megaterium* (TyrBm; a soil bacterium), which has an exceptionally high activity in water-miscible organic solvents[23] and does not appear to require the presence of a caddie protein for activity. Here we describe the determination of the crystal structures of this tyrosinase (TyrBm) under different conditions up to a maximal resolution of 2.0 Å. The crystals contain a dimer of the enzyme in the asymmetric unit, and the enzyme is fully active in crystal. The structure of a site-specific mutant, recently shown to have an increased monophenolase/diphenolase activity ratio,[24] was determined as well. This work identifies additional features and residues that are important for this enzyme's catalytic cycle and reveals that these activities may require movement in the positions of the active-site copper ions.

Results and Discussion

Overall structure of TyrBm in the two crystal forms

The structures of TyrBm were determined at a resolution of 2.0–2.3 Å. The two TyrBm monomers in the asymmetric unit are associated in a homodimeric structure, are ellipsoid in shape, and have dimensions of 45 Å × 25 Å × 80 Å (Fig. 1). α-Helices are the main secondary structure element of TyrBm, with the copper center located at the core of a four-helical bundle, which is conserved in all type 3 copper enzymes.[11,14–16,18,19] Each copper ion is coordinated by three His residues, which project out from the four surrounding helices (α2, α3, α7, and α8) and by one loop. CuA is coordinated by His42 (α2), His69 (α3), and His60, which is located on a large loop intervening between these two helices. The second copper ion CuB is coordinated by His204, His208 (both on α7), and His231 (α8). In all type 1 crystal structures described below and obtained in the presence of Zn ions (TyrBm1, TyrBm1_*Cu*, TyrBm1_*mut*, and TyrBm1_*koj*), two copper ions were observed on each monomer. In contrast, in type 2 crystal structures (TyrBm2 and TyrBm2_*CuB**) crystallized in the absence of Zn, only copper ion CuA was identified (see the text).

TyrBm is a dimer

This is the first determined structure of a prokaryote tyrosinase that does not contain a caddie protein and appears to form a dimer. The dimer is formed *via* two 2-fold symmetry axes; thus, the substrate-binding pockets face alternate directions (Fig. 1) and are not obscured by other symmetry-related monomers in the crystal lattice. The dimer interface contains interactions between symmetry-related α2-helices and two large loops. The major dimer-forming contacts include Trp41-Tyr267 and Arg37-Asn270 (Fig. 1). The hydrophobic interactions between the two symmetry-related Trp41 and Tyr267 couples, along with residues Trp269 and Phe48, form a tight hydrophobic center (~3.5 Å between interacting residues) composed of both van der Waals interactions and π–π stacking interactions situated at the heart of the dimer

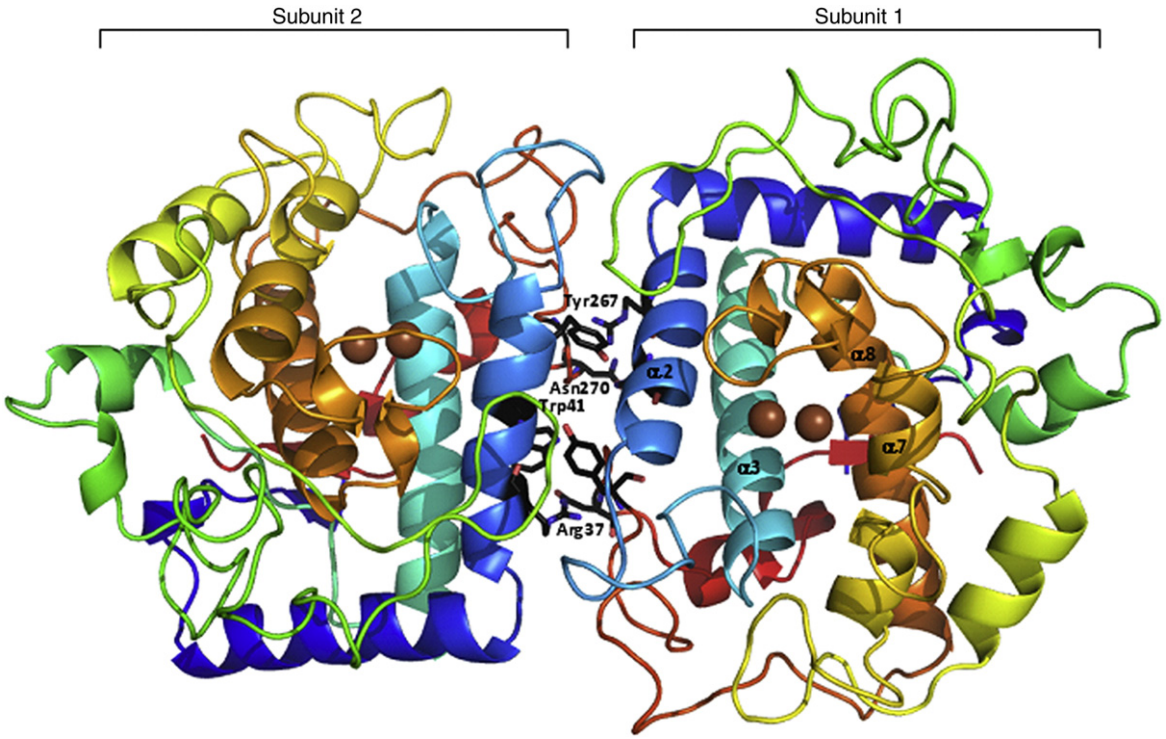

Fig. 1. Overview of TyrBm structure. The dimer structure of TyrBm is presented; both subunits (subunit 1 on the right and subunit 2 on the left) are presented in an N-terminal to C-terminal spectrum. Copper ions in the active site are presented in brown. The dimer-forming contacts in each subunit, Trp41-Tyr267 and Arg37-Asn270, are shown in black. The four main helices, from which the His residues coordinating the copper ions project, are presented in subunit 1: α2 in light blue, α3 in cyan, α7 in dark yellow, and α8 in orange. The structure presented is that of TyrBm1 (a type 1 crystal) crystallized in the presence of Zn ions. The overall structures of all other crystal structures described here are nearly identical. All figures presented in this work were generated using PyMOL (http://www.pymol.org/).

interface surface. Both of these residues (Trp41 and Tyr267) are chemically nonconserved in the TyrSc protein (Thr37 and Lys252, respectively); indeed, in the TyrSc protein, this surface is solvent exposed. It would certainly be energetically favorable to bury these four aromatic residues within the interface rather than expose them on the surface.

TyrBm was formerly reported to be a monomer in solution.[23] Reanalysis of the purified soluble protein by high-resolution size-exclusion chromatography revealed the presence of two species of TyrBm [a monomer (~35 kDa) and a dimer (~70 kDa)], and elevation of the protein concentration appears to shift the equilibrium to the dimeric species in a solution. A similar behavior was reported for enzymes such as yeast hexokinase[25] and NS3 helicase from hepatitis C[26] for which a concentration-dependent equilibrium exists between monomers and higher oligomers. The buried surface area at the interface between associating monomers is 1045 Å^2, as calculated by PROTROP‡. This value is considered marginal in terms of dimer classification,[27] although actual contacts within the interface must also be taken into account. The dimer obtained in the asymmetric unit is also consistent with a biologically relevant dimer obtained by analysis with PISA§. Therefore, we propose that the structure obtained is a biologically relevant dimer. Since TyrBm is secreted from the cells into the surrounding soil, there may be a difference in the oligomeric form of the enzyme *in vivo* and outside the cell.

TyrBm is active in crystal

Crystals soaked in L-tyrosine for over 48 h turned brown (Fig. 2), indicating oxidation of the substrate into *o*-quinone and accumulation of dopachrome. The rate-limiting step of the reaction in crystal may be the availability of molecular oxygen. The structure of a brown crystal (data collected a few weeks after color formation) was determined and found to be identical with that of a crystal not exposed to L-tyrosine. Thus, the activated enzyme apparently

‡ http://www.bioinformatics.sussex.ac.uk/protorp/

§ http://www.ebi.ac.uk/msd-srv/prot_int/pistart.html

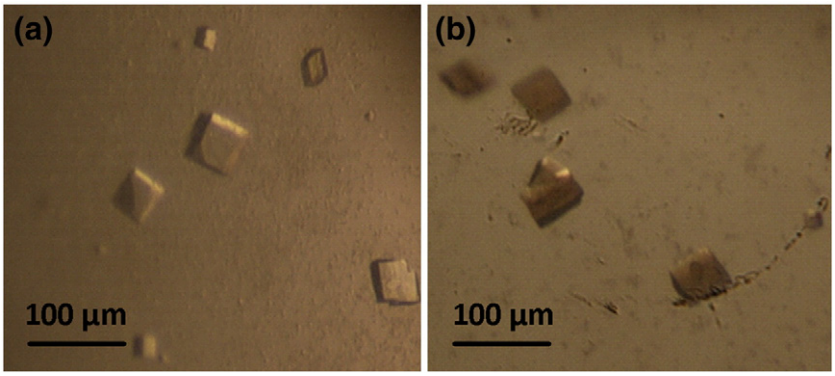

Fig. 2. TyrBm crystals have monooxygenase activity. (a) TyrBm monoclinic (type 2) crystals obtained in drops containing 18% polyethylene glycol 8000 and 0.1 M cacodylic acid (pH 5.6) at 20 °C after 14–21 days. (b) Crystals were soaked in 0.5 mM L-tyrosine and turned brown after 48 h.

returned to the basic met form after all of the substrate had been oxidized. We can thus propose that the structures we present here are those of active enzyme molecules. We were not able to crystallographically visualize the product (dopachrome) within the active site of the crystals, indicating that the product has reduced affinity for the enzyme active site.

Plasticity in copper ion occupancy and binding mode

In the process of data collection from crystals grown under different conditions, we identified TyrBm structures with different copper occupancies and positions. The structure of TyrBm1 bears two copper ions 3.5 Å apart, with one bridging solvent molecule designated as water (Fig. 3a). We suggest that this structure represents the met form of TyrBm, similar to the met I form of TyrSc [Protein Data Bank (PDB) code 2ZMX][11] and to the met form of catechol oxidase from *Ipomoea batatas* (PDB code 1BT3).[14] Han *et al.* showed that Zn ions inactivated mushroom tyrosinase in a mixed-type manner and caused conformational changes as reflected by thermodynamic parameters.[28] Indeed, increasing concentrations of ZnAc were found to inhibit TyrBm activity as well (results not shown). Zn ions could bind to histidine or cysteine residues at different protein locations, or may even substitute the Cu ions in the active site. In the TyrBm structures reported here, Zn ions were observed bound (such as to His13 or His279) in a number of locations in the enzyme. It could not be ruled out that in protein molecules crystallized in the presence of Zn ions (type 1 structures), heterogeneity of Cu and Zn ions is observed at the active site. A similar occurrence was reported for the crystal structure of the mammalian serine protease Tonin, in which Zn ions, introduced to improve crystal formation, were bound in the active site and inhibited activity.[29] In the present study, we showed activity in crystal, indicating the presence of active-site Cu, and not only of Zn from the crystallization liquor.

The structure of TyrBm2 (Fig. 3b), crystallized in the absence of Zn ions (type 2), has one water molecule bound to CuA and lacks CuB. Based on this result, it is speculated that the binding of CuB may be labile, although its surrounding ligation sphere is more conserved.[22] Thus, in the presence of an excess of Zn ions, such as in type 1 crystal structures, CuB could possibly be replaced by a Zn ion. CuA, however, is present in all of the structures determined. The structure of TyrBm2_*CuB** (Fig. 3c) is of a type 2 crystal soaked in L-dihydroxyphenylalanine (L-DOPA) for 30 min. The soak was not long enough to see dopachrome or melanin formation, but a change in the copper occupancy was observed. In this structure, CuA was present in both subunits, while CuB was observed in subunit 1; we estimated its occupancy at 40%. This implies that in the crystals, this fraction of TyrBm had a bound CuB ion, indicating copper stabilization perhaps due to the aforementioned experimental conditions. This phenomenon is described here for the first time for type 3 copper proteins and demonstrates the dynamics of copper occupancy in TyrBm. Matoba *et al.* suggested that the incorporation of copper into TyrSc is mediated by a caddie protein (ORF378) that covers the active site and binds copper ions through a number of His residues on the molecule.[11] TyrBm has no such helper protein, and its active site is relatively exposed. In *B. megaterium*, the tyrosinase is secreted to the surrounding medium as in tyrosinases from *Streptomyces*, where they are involved in extracellular melanin production.[1] The difference in copper accumulation could have developed as a result of the different environments to which the enzyme is secreted and its abundance or deficiency in copper.

We were also able to identify heterogeneity in the binding of CuA. A structure (TyrBm1_*Cu*; Fig. 3d)

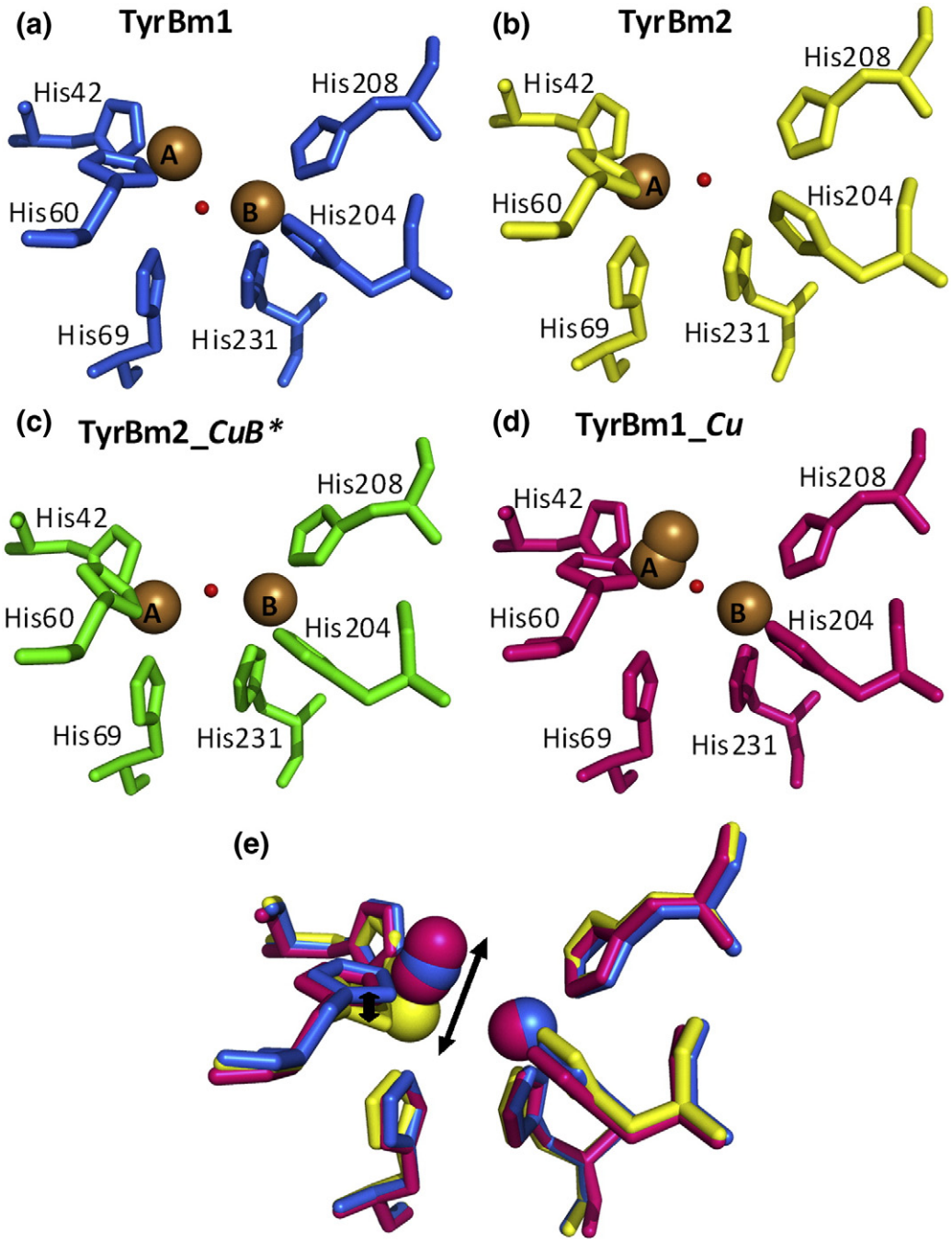

Fig. 3. Positions and occupation of copper in different TyrBm structures. (a) The active sites of TyrBm1 (blue) crystallized in the presence of Zn. (b) TyrBm2 (yellow) crystallized in the absence of Zn. (c) TyrBm2_*CuB** (green) crystallized in the absence of Zn ions and soaked for 30 min in 0.5 mM L-DOPA (the active site of subunit 1 is shown). (d) TyrBm1_*Cu* (pink) crystallized in the presence of Zn and soaked in 1 mM $CuSO_4$ for 30 min. (e) Superposition of the three structures shown in (a), (b), and (d), with the narrow arrow showing a 2.0-Å distance between the two farthest CuA positions and with the wide arrow showing a concomitant 1.0-Å movement in His60. Copper ions are depicted in brown (a–d) and in the color of the structure (e), where CuA is shown on the left and CuB is shown on the right. Water molecules are shown in red. In each structure, the occupation and positioning of copper vary (see the text).

was obtained by soaking a type 1 crystal in 1 mM $CuSO_4$ for 30 min, and CuA can be seen in the active site at two overlapping positions (with occupancies of ~50% each). The two overlapping positions of CuA are 0.5 Å apart (Fig. 3d). The positions of CuA in TyrBm1 and TyrBm2 are separated by 1.5 Å,

accompanied by a concomitant 1-Å change in the positions of the ligating residues His60 and His42. Superposition of the three structures reveals a profile of CuA movement by as much as 2 Å, directed away from His69 (Fig. 3e). Furthermore, in TyrBm1, there is weak electron density between His69 and the designated copper position, which is not consistent with a solvent molecule. This additional electron density may represent an additional minor CuA binding mode in TyrBm1, analogous with its position in TyrBm2. As there is no thioether bond stabilizing His60 (as in PDB code 1BT3),[14] the simultaneous movements of His60 and CuA are possible in tyrosinases. The movement of CuA seems to be affected by the abundance in copper, and CuB is lost when copper is limited (TyrBm2); only a single binding mode was identified when copper was in excess. The presence of CuA under all conditions indicates tighter binding (perhaps by the existence of multiple binding modes) and suggests that it has greater overall importance to the enzyme, perhaps not only for activity but also for structural maintenance.

Comparison to TyrSc and other type 3 copper proteins

Type 3 copper proteins, to which TyrBm belongs, compose a family of proteins with varying structures, amino acid sequences, and functions that possess a practically identical active site. This conundrum has been the focus of many studies, with the recent structural studies providing major contributions to our understanding of the functional aspects of this family. Catechol oxidase and hemocyanin structures were determined more than a decade ago, and the first structure of a tyrosinase was determined more recently.[11,14,16,18] In hemocyanin oxygen carriers, no enzymatic activity has been identified; indeed, the active site is blocked by the protein itself. A leucine (Leu2830) or phenylalanine (Phe49) residue extends into the substrate binding site.[16,18] Therefore, no substrate can reach the active site; unless these residues are removed, no activity can be obtained. This was substantiated by the work of Decker and Rimke in which hemocyanin from tarantula was turned into a weak phenoloxidase after the *in vitro* cleavage of an N-terminal peptide, including a conserved Phe49 that serves as an allosteric trigger during the oxygenation process.[30] Recently, SDS was shown to induce phenoloxidase activity in scorpion hemocyanin by causing the covering domain to twist away and expose the active site.[31] The blocking residue is considered the "placeholder."

A similar placeholder was observed in the TyrSc structure in complex with a caddie protein. Tyr98 of the caddie protein is oriented in a fashion similar to that of Phe49 in hemocyanin from *Limulus*, blocking the active site.[20] The tyrosine residue is just far enough from the dicopper center for it not be hydroxylated itself. Detachment of the caddie protein will enable the exposure of the active site to phenolic substrates and monophenolase or diphenolase activity to occur. In the structure of catechol oxidase from *I. batatas*, the lack of monophenolase activity was attributed to the presence of Phe261 near CuA.[14] This residue was also considered to be a gatekeeper residue, controlling the entrance to the active site similar to the placeholders described in other proteins, since a structure determined with an inhibitor (phenylthiourea) in the active site shows a significant movement of the residue.[32]

As mentioned earlier, the active site of TyrBm is relatively exposed, and no "placeholder" residues were identified within the active site. However, Val218, situated on a loop adjacent to CuA, extends into the active site in a fashion similar to Phe261 in catechol oxidase (Fig. 4a).[16] Since valine is far less bulky than phenylalanine, it does not prevent the hydroxylation of monophenols by TyrBm, which apparently occurs on CuA. The homologous loop in TyrSc is shorter and located farther from the active site, with Gly204 in the Val218 position (Fig. 4b).[11] Val218 can therefore be proposed as a modified gatekeeper residue, controlling the entrance to the active site of TyrBm; as for Phe261 in catechol oxidase, it may move as a substrate penetrates into the active site. Movement of Val218 may help direct the substrate correctly into the active site.

Another residue that we have identified as having a possible role in substrate docking is Arg209. It is positioned in proximity to the entrance of the active site, on helix α6 adjacent to His208, which coordinates CuB. In subunit 1 of TyrBm1, two conformations of this residue were observed, indicating its flexibility (Fig. 5a). The different conformations are stabilized by hydrogen bonds with adjacent residues and allow the expansion or contraction of the active-site volume. The movements in the position of Arg209 may also cause pK_a changes in the area, which could have catalytic importance in the presence of a substrate (see the text).

Insights into the catalytic mechanism of tyrosinase

Although tyrosinase and its related proteins have been intensively studied, its catalytic mechanism is still a subject of debate due to its complexity, the existence of two catalytic activities at the same active site, and the apparent lag period associated with monophenolase activity.[7] Based on the lack of monophenolase activity in catechol oxidase (which has a large aromatic residue blocking CuA), it has been suggested that in tyrosinases (lacking this blocking residue), monophenols bind to CuA and

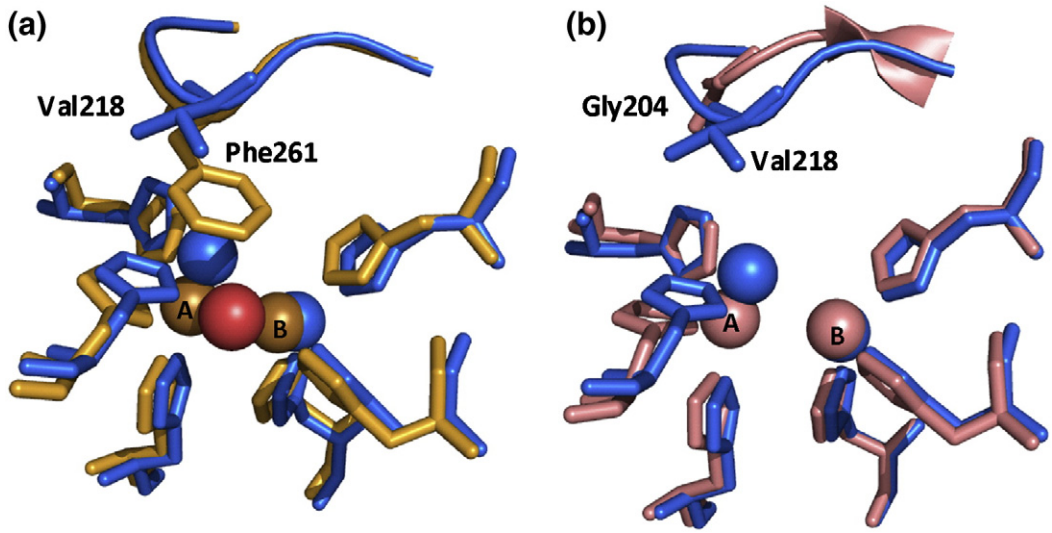

Fig. 4. Superposition of the active sites of TyrBm and related type 3 copper proteins. (a) TyrBm1 (blue) superimposed onto the catechol oxidase from *I. batatas* (orange; PDB code 1BT3). Phe261 shields CuA, preventing the ability of catechol oxidase to hydroxylate monophenols. The red sphere represents a water molecule. (b) TyrBm1 (blue) and TyrSc (light pink; PDB code 1WX2). In TyrBm, Val218 reaches into the active site above CuA, whereas in TyrSc, there is a shorter and tighter loop with Gly204 in the homologous position.

o-diphenols bind to CuB.[5,6,32] The evidence provided by the recently determined structure of TyrSc has led to two possible hydroxylation mechanisms, as proposed by Matoba *et al.*[11] and Decker *et al.*[20] Matoba *et al*. suggested that the deprotonated monophenol binds to CuB, followed by the addition of oxygen to the ring in ortho position through a connection to CuA, enabled by the release of the flexible His54. This residue has also been suggested to be involved in the deprotonation of the monophenolic substrate.[7,19] In catechol oxidase, the mechanism is not possible because of the fixed conformation of the corresponding His residue. Decker *et al.* suggested that the monophenol substrate is oriented towards CuA through hydrophobic interactions with His194 (His208 in TyrBm), in analogy to the orientation of Tyr98 (in TyrSc).[20] Hydroxylation occurs *via* an electrophilic substitution mechanism[5] while the substrate is positioned in trans to His63 (His69 in TyrBm). Olivares *et al.*[6] and Olivares and Solano[7] also proposed that monophenols dock to CuA but *o*-diphenols dock to CuB, based on site-specific mutations of mouse tyrosinase, suggesting a similar mechanism.

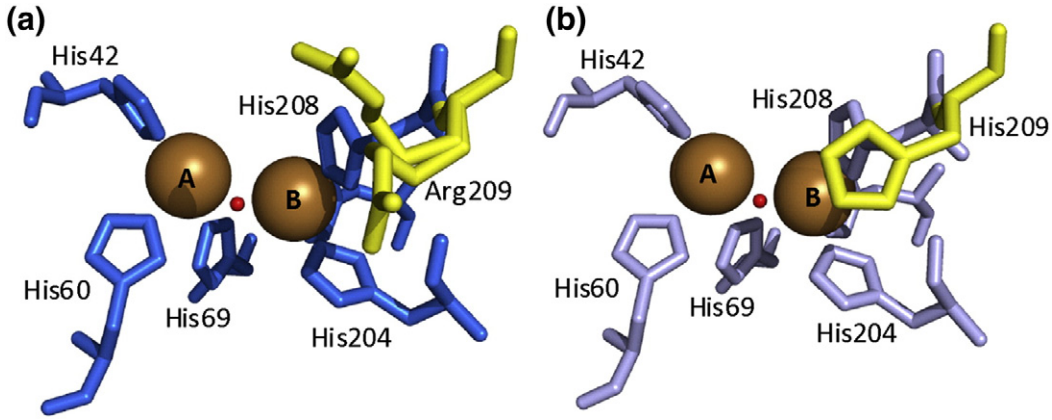

Fig. 5. The active sites of wild-type TyrBm and variant R209H. (a) The active site of wild-type TyrBm (TyrBm1) is presented in blue, and the two conformations of Arg209 identified in the electron density maps are presented in yellow. (b) The active site of variant R209H (structure of TyrBm1_*mut*) and residue His209 are shown in light blue and yellow, respectively.

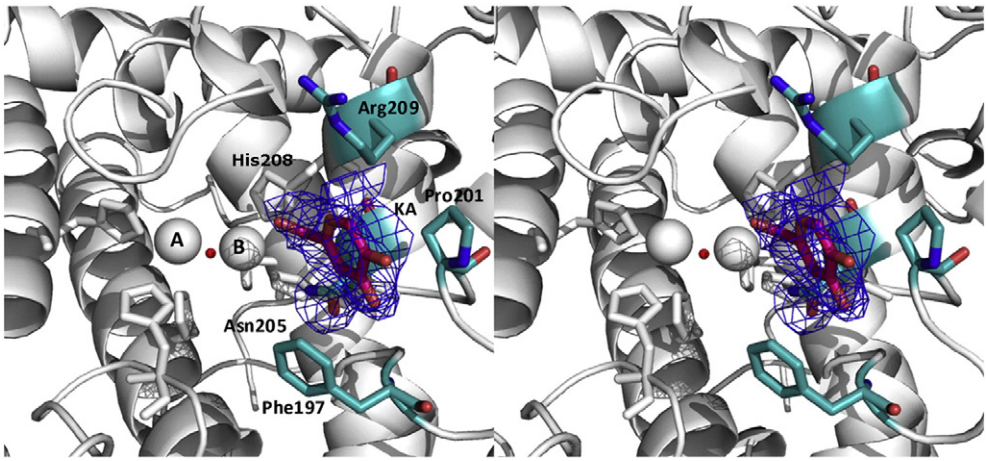

Fig. 6. The structure of TyrBm in complex with kojic acid identifies an unexpected binding mode. Stereo view of kojic acid (KA; magenta), which is in the entrance to the active site of TyrBm (structure of TyrBm1_*koj*; His residues are in white) and is stabilized by residues in the active-site area (light blue). KA is 7 Å away from the copper center. The omit $F_o - F_c$ electron density map (blue wire; 1σ) is overlaid onto the KA model.

The study presented here provides additional structural evidence that supports the latter mechanism. The crystal structure of TyrBm suggests that His208 of CuB is in a position to orient a substrate towards CuA, as suggested by Decker *et al.* (Fig. 5a). The location of His60 on a loop allows for positional flexibility, and its proximity to CuA correlates with the hypothesis that it is responsible for the deprotonation of the monophenolic substrate. In addition, the flexible and small Val218 residue situated near CuA (Fig. 4a) allows monophenolase activity to occur. This suggests that monophenol substrates are oriented towards CuA. Furthermore, the movement of CuA towards the protein surface supports its conspicuous role in the first stages of catalysis.

We have recently identified, by directed evolution, a residue that influences the selectivity of TyrBm.[24] The variant R209H exhibited a monophenolase/diphenolase activity ratio that is 2.6-fold higher than that of the wild-type enzyme. It was suggested that the imidazole group of the newly introduced histidine residue obstructs the entrance to the active site, thus interfering with the binding of L-DOPA to CuB. At the same time, access of L-tyrosine to the CuA site is less hindered, as was demonstrated from the higher k_{cat} value of the mutant with this substrate. These results support the hypothesis that tyrosine and L-DOPA bind differently within the active site. We have determined the structure of R209H to a resolution of 2.3 Å (TyrBm1_*mut*). In the structure, His209 can be seen to shield CuB and to obstruct the entrance to the active site (Fig. 5b). As shown in the structures of wild-type and mutant TyrBm, Arg209 is flexible, while the histidine is rigid. This structural evidence further supports the hydroxylation mechanism in which a monophenol substrate docks to CuA.

Structure of TyrBm with the tyrosinase inhibitor kojic acid

Kojic acid (5-hydroxy-2-(hydroxymethyl)-*g*-pyrone) is a fungal metabolite produced by many species of *Aspergillus* and *Penicillium*.[33] It is a good chelator of transition metal ions and a good scavenger of free radicals.[33] Kojic acid is an inhibitor of tyrosinases of various bacteria, mushrooms, plants, and arthropods, and is currently used as a skin-whitening agent and as a food additive to prevent enzymatic browning.[34] The inhibition is competitive for monophenolase activity and has a mixed inhibitory effect on the diphenolase activity of mushroom tyrosinase.[34] The suggested mechanism of inhibition is by the chelation of copper in the active site. Moreover, kojic acid is able to reduce *o*-quinone to *o*-diphenol to prevent the final pigment formation.

We determined the structure of TyrBm with bound kojic acid (TyrBm1_*koj*; Fig. 6), the first tyrosinase structure determined with a bound ligand. As opposed to the previously suggested binding modes in which kojic acid is bound to the copper ions in a bidentate fashion through its ortho-positioned hydroxyl and carbonyl groups,[35] it is oriented with the hydroxymethyl towards the active site at a relatively far distance of 7 Å. The molecule appears in both subunits of TyrBm in identical positions and is bound strongly by interactions with residues in the active-site entrance: Phe197, Pro201, Asn205, and Arg209. Furthermore, kojic acid is oriented similarly to the placeholder Tyr98 of the TyrSc caddie protein, although not quite as close to the active site. Thus, the position and orientation of kojic acid cause an obstruction of the active site, which could be one mechanism of inhibition. A docking study of kojic acid in the active site of

Table 1. Data collection and refinement statistics

Structure name (PDB code)	Structure name (PDB code)					
	TyrBm1 (3NM8)	TyrBm2 (3NQ0)	TyrBm2_*CuB** (3NTM)	TyrBm1_*Cu* (3NPY)	TyrBm1_*mut* (3NQ5)	TyrBm1_*koj* (3NQ1)
X-ray data collection						
Space group	$P2_12_12_1$	$P2_1$	$P2_1$	$P2_12_12_1$	$P2_12_12_1$	$P2_12_12_1$
Unit cell parameters						
a (Å)	51.2	47.8	46.0	49.5	49.1	51.4
b (Å)	84.5	78.7	78.4	82.1	80.9	83.6
c (Å)	146.3	85.6	74.6	146.7	147.1	146.2
α (°)	90	90	90	90	90	90
β (°)	90	105.3	101.6	90	90	90
γ (°)	90	90	90	90	90	90
Resolution range	50–2.0	40–2.2	40–2.3	50–2.2	50–2.3	50–2.3
Observed reflections	155,304	60,695	46,496	154,754	53,570	52,574
Unique reflections	42,991	29,606	22,077	31,000	25,173	24,154
$I/\sigma(I)$[a]	7.7 (1.6)	8.3 (2.4)	10.5 (4.4)	13.0 (3.1)	7.1 (2.6)	9.1 (2.5)
R_{merge}[a b]	0.09 (0.67)	0.10 (0.33)	0.06 (0.19)	0.07 (0.43)	0.08 (0.24)	0.09 (0.29)
Completeness[a]	98.1 (98.4)	95.1 (87.3)	95.5 (94.0)	98.5 (95.5)	94.1 (81.7)	84.7 (72.8)
Multiplicity[a]	3.6 (3.8)	2.1 (1.9)	2.1 (2.0)	5.0 (5.2)	2.1 (1.8)	2.2 (1.9)
Refinement						
R (%)/R_{free} (%)[c]	21.9/27.2	24.3/29.2	19.3/28.9	25.5/27.8	21.6/30.9	22.8/26.2
Amino acids	568	559	561	565	566	564
Total number of nonhydrogen atoms	5021	4759	4667	4827	4961	4800
Number of water molecules	340	159	236	172	249	208
Number of copper ions	4 (3.6)[d]	2	3 (3.2)[d]	4 (3.4)[d]	4 (3.6)[d]	4 (3.5)[d]
Number of Zn ions	7	0	0	8	10	13
Average *B*-factor (Å), protein atoms	32.8	20.0	21.7	41.3	28.8	26.6
r.m.s.d.						
Bond length (Å)	0.009	0.012	0.011	0.016	0.011	0.012
Bond angle (°)	1.4	1.5	1.3	1.5	1.3	1.4
Ramachandran plot						
Favored regions (%)	95.6	95.1	94.2	94.8	93.2	95.0
Outliers (%)	0.0	0.7	1.1	0.9	1.4	0.4

[a] Values in parentheses are for the last shell.
[b] $R_{merge} = \sum_{hkl}\sum_i |I_i(hkl) - \langle I(jkl)\rangle| / \sum_{hkl}\sum_i I_i(hkl)$, where I is the observed intensity, and $\langle I\rangle$ is the mean value of I.
[c] $R/R_{free} = \sum_{hkl}||F_{obs}| - |F_{calc}||/\sum_{hkl}|F_{obs}|$, where R and R_{free} are calculated using test reflections, respectively. The test reflections (10%) were held aside and not used during the entire refinement process.
[d] Distance (Å) between copper ions when both CuA and CuB are present.

tyrosinase from *Streptomyces* predicted π–π interactions with His194 (His208 in TyrBm) and orientation of the hydroxymethyl moiety towards the dicopper center.[36] The location of kojic acid in TyrBm presented here could be an intermediate binding site—but one that has significant binding strength. Further movement into the active site could require changes in protein conformation occurring in the presence of substrate. The full mechanism of kojic acid inhibition is still far from understood, but this structure presents new evidence for the possible orientation of ligands in the active site of tyrosinases.

Materials and Methods

Expression, purification, and crystallization

A tyrosinase-producing *B. megaterium* was isolated by our laboratory from soil samples, and the gene encoding for the tyrosinase was cloned into *Escherichia coli* BL21, expressed, purified, and crystallized as previously described.[23,37] Briefly, two different crystallization conditions were obtained using commercial crystal screen kits in the presence and in the absence of 0.2 M Zn^{2+}, resulting in two different crystal types: rods (type 1) and cubes (type 2). The enzyme's molecular weight in solution was determined by size-exclusion chromatography (Superdex 200 HR 10/30; GE Healthcare, Uppsala, Sweden) at a protein concentration range of 2–5 mg ml^{-1} and under buffer conditions of 50 mM Tris–HCl (pH 7.5) and 100 mM NaCl.

Crystal activity

Mature crystals were soaked in 0.5 mM L-tyrosine (Sigma-Aldrich, Israel) for 48 h to test activity. As opposed to L-DOPA, L-tyrosine in solution does not oxidize spontaneously; thus, the hanging drop remained clear, and the reaction occurred only inside the crystals, turning them brown.

The TyrBm mutant R209H

The mutant R209H was obtained by directed evolution, as described previously.[24] Briefly, mutagenesis was

introduced using error-prone PCR, and a high-throughput assay for enhanced activity on tyrosinase substrates was used to locate mutants that have higher activity on L-tyrosine and lower activity on L-DOPA compared to wild type. Purification and crystallization steps (in the presence of ZnAc) were identical with those performed on the wild type, and rod-shaped crystals similar to those of the wild type were obtained. For visualization of ligand binding modes, a fully grown crystal was incubated in 3 mM kojic acid (Sigma-Aldrich), a well-characterized tyrosinase inhibitor, in artificial mother liquor. After 5 min, the crystal was mounted on a loop and frozen.

Data collection and structure determination

X-ray diffraction data were collected at beamlines ID14-1 and ID23-1 of the European Synchrotron Radiation Facility (Grenoble, France). All data were indexed, integrated, scaled, and merged using Mosflm and Scala.[38] The structure of TyrBm in type 1 crystals was solved by molecular replacement using Phaser[39] and the coordinates of TyrSc (PDB code 1WX2), which has a 40% sequence identity to TyrBm. A single solution was obtained for two monomers in the asymmetric unit. Refinement was performed using CNS,[40] PHENIX,[41] and Refmac5.[42,43] Manual model building, real-space refinement, and structure validation were performed using Coot.[44] The structure of TyrBm in type 2 crystals was solved by molecular replacement using the coordinates of the TyrBm structure from type 1 crystals. Data collection, phasing, and refinement statistics are presented in Table 1.

PDB accession numbers

The coordinates and structure factors of TyrBm in different states have been deposited in the RCSB PDB under accession codes 3NM8, 3NPY, 3NQ0, and 3NTM. The code for the TyrBm variant R209H is 3NQ5, and that for TyrBm with kojic acid is 3NQ1.

Acknowledgements

This work was supported by the Israel Science Foundation founded by the Israel Academy of Sciences and Humanities (grant 535/07).

References

1. Claus, H. & Decker, H. (2006). Bacterial tyrosinases. *Syst. Appl. Microbiol.* **29**, 3–14.
2. Burton, S. G. (2003). Oxidizing enzymes as biocatalysts. *Trends Biotechnol.* **21**, 543–549.
3. Selinheimo, E., NiEidhin, D., Steffensen, C., Nielsen, J., Lomascolo, A., Halaouli, S. *et al.* (2007). Comparison of the characteristics of fungal and plant tyrosinases. *J. Biotechnol.* **130**, 471–480.
4. Martinez, M. V. & Whitaker, J. R. (1995). The biochemistry and control of enzymatic browning. *Trends Food Sci. Technol.* **6**, 195–200.
5. Decker, H. & Tuczek, F. (2000). Tyrosinase/catecholoxidase activity of hemocyanins: structural basis and molecular mechanism. *Trends Biochem. Sci.* **25**, 392–397.
6. Olivares, C., Garcia-Borron, J. C. & Solano, F. (2002). Identification of active site residues involved in metal cofactor binding and stereospecific substrate recognition in mammalian tyrosinase. Implications to the catalytic cycle. *Biochemistry*, **41**, 679–686.
7. Olivares, C. & Solano, F. (2009). New insights into the active site structure and catalytic mechanism of tyrosinase and its related proteins. *Pigm. Cell Melanoma Res.* **22**, 750–760.
8. Decker, H., Schweikardt, T., Nillius, D., Salzbrunn, U., Jaenicke, E. & Tuczek, F. (2007). Similar enzyme activation and catalysis in hemocyanins and tyrosinases. *Gene*, **398**, 183–191.
9. van Gastel, M., Bubacco, L., Groenen, E. J. J., Vijgenboom, E. & Canters, G. W. (2000). EPR study of the dinuclear active copper site of tyrosinase from *Streptomyces antibioticus*. *FEBS Lett.* **474**, 228–232.
10. Fenoll, L. G., Penalver, M. J., Rodriguez-Lopez, J. N., Varon, R., Garcia-Canovas, F. & Tudela, J. (2004). Tyrosinase kinetics: discrimination between two models to explain the oxidation mechanism of monophenol and diphenol substrates. *Int. J. Biochem. Cell Biol.* **36**, 235–246.
11. Matoba, Y., Kumagai, T., Yamamoto, A., Yoshitsu, H. & Sugiyama, M. (2006). Crystallographic evidence that the dinuclear copper center of tyrosinase is flexible during catalysis. *J. Biol. Chem.* **281**, 8981–8990.
12. Itoh, S. & Fukuzumi, S. (2007). Monooxygenase activity of type 3 copper proteins. *Acc. Chem. Res.* **40**, 592–600.
13. van Holde, K. E., Miller, K. I. & Decker, H. (2001). Hemocyanins and invertebrate evolution. *J. Biol. Chem.* **276**, 15563–15566.
14. Klabunde, T., Eicken, C., Sacchettini, J. C. & Krebs, B. (1998). Crystal structure of plant catechol oxidase containing a dicopper center. *Nat. Struct. Biol.* **5**, 1084–1090.
15. Virador, V. M., Reyes Grajeda, J. P., Blanco-Labra, A., Mendiola-Olaya, E., Smith, G. M., Moreno, A. & Whitaker, J. R. (2010). Cloning, sequencing, purification, and crystal structure of Grenache (*Vitis vinifera*) polyphenol oxidase. *J. Agric. Food Chem.* **58**, 1189–1201.
16. Cuff, M. E., Miller, K. I., van Holde, K. E. & Hendrickson, W. A. (1998). Crystal structure of a functional unit from octopus hemocyanin. *J. Mol. Biol.* **278**, 855–870.
17. Gaykema, W. P. J., Hol, W. G. J., Vereijken, J. M., Soeter, N. M., Bak, H. J. & Beintema, J. J. (1984). 3.2 Å structure of the copper-containing, oxygen-carrying protein *Panulirus interruptus* haemocyanin. *Nature*, **309**, 23–29.
18. Hazes, B., Magnus, K. A., Bonaventura, C., Bonaventura, J., Dauter, Z., Kalk, K. H. & Hol, W. G. (1993). Crystal structure of deoxygenated *Limulus polyphemus* subunit II hemocyanin at 2.18 Å resolution: clues for a mechanism for allosteric regulation. *Protein Sci.* **2**, 597–619.
19. Li, Y., Wang, Y., Jiang, H. & Deng, J. (2009). Crystal structure of *Manduca sexta* prophenoloxidase provides insights into the mechanism of type 3 copper enzymes. *Proc. Natl Acad. Sci. USA*, **106**, 17002–17006.

20. Decker, H., Schweikardt, T. & Tuczek, F. (2006). The first crystal structure of tyrosinase: all questions answered? *Angew. Chem. Int. Ed. Engl.* **45**, 4546–4550.
21. Magnus, K. A., Ton-That, H. & Carpenter, J. E. (1994). Recent structural work on the oxygen transport protein hemocyanin. *Chem. Rev.* **94**, 727–735.
22. Eicken, C., Krebs, B. & Sacchettini, J. C. (1999). Catechol oxidase—structure and activity. *Curr. Opin. Struct. Biol.* **9**, 677–683.
23. Shuster, V. & Fishman, A. (2009). Isolation, cloning and characterization of a tyrosinase with improved activity in organic solvents from *Bacillus megaterium*. *J. Mol. Microbiol. Biotechnol.* **17**, 188–200.
24. Shuster Ben-Yosef, V., Sendovski, M. & Fishman, A. (2010). Directed evolution of tyrosinase for enhanced monophenolase/diphenolase activity ratio. *Enzyme Microb. Technol.* **47**, 372–376.
25. Shill, J. P., Peters, B. A. & Neet, K. E. (1974). Monomer–dimer equilibriums of yeast hexokinase during reacting enzyme sedimentation. *Biochemistry*, **13**, 3864–3871.
26. Jennings, T. A., Mackintosh, S. G., Harrison, M. K., Sikora, D., Sikora, B., Dave, B. *et al.* (2009). NS3 helicase from the hepatitis C virus can function as a monomer or oligomer depending on enzyme and substrate concentrations. *J. Biol. Chem.* **284**, 4806–4814.
27. Ponstingl, H., Henrick, K. & Thornton, J. M. (2000). Discriminating between homodimeric and monomeric proteins in the crystalline state. *Proteins Struct. Funct. Genet.* **41**, 47–57.
28. Han, H. Y., Zou, H. C., Jeon, J. Y., Wang, Y. J., Xu, W. A., Yang, J. M. & Park, Y. D. (2007). The inhibition kinetics and thermodynamic changes of tyrosinase *via* the zinc ion. *Biochim. Biophys. Acta*, **1774**, 822–827.
29. Fujinaga, M. & James, M. N. G. (1987). Rat submaxillary gland serine protease, Tonin: structure solution and refinement at 1.8 Å resolution. *J. Mol. Biol.* **195**, 373–396.
30. Decker, H. & Rimke, T. (1998). Tarantula hemocyanin shows phenoloxidase activity. *J. Biol. Chem.* **273**, 25889–25892.
31. Cong, Y., Zhang, Q., Woolford, D., Schweikardt, T., Khant, H., Dougherty, M. *et al.* (2009). Structural mechanism of SDS-induced enzyme activity of scorpion hemocyanin revealed by electron cryomicroscopy. *Structure*, **17**, 749–758.
32. Gerdemann, C., Eicken, C. & Krebs, B. (2002). The crystal structure of catechol oxidase: new insight into the function of type-3 copper proteins. *Acc. Chem. Res.* **35**, 183–191.
33. Kim, Y. J. & Uyama, H. (2005). Tyrosinase inhibitors from natural and synthetic sources: structure, inhibition mechanism and perspective for the future. *Cell Mol. Life Sci.* **62**, 1707–1723.
34. Chang, T. S. (2009). An updated review of tyrosinase inhibitors. *Int. J. Mol. Sci.* **10**, 2440–2475.
35. Battaini, G., Monzani, E., Casella, L., Santagostini, L. & Pagliarin, R. (2000). Inhibition of the catecholase activity of biomimetic dinuclear copper complexes by kojic acid. *J. Biol. Inorg. Chem.* **5**, 262–268.
36. Nithitanakool, S., Pithayanukul, P., Bavovada, R. & Saparpakorn, P. (2009). Molecular docking studies and anti-tyrosinase activity of Thai mango seed kernel extract. *Molecules*, **14**, 257–265.
37. Sendovski, M., Kanteev, M., Shuster, V., Adir, N. & Fishman, A. (2010). Primary X-ray crystallographic analysis of a bacterial tyrosinase from *Bacillus megaterium*. *Acta Crystallogr. Sect. F*, **66**, 1101–1103.
38. Leslie, A. G. W. (1992). Recent changes to the MOSFLM package for processing film and image plate data. *Joint CCP4+ ESF-EAMCB Newsletter on Protein Crystallography*, **26**.
39. McCoy, A. J. (2007). Solving structures of protein complexes by molecular replacement with Phaser. *Acta Crystallogr. Sect. D*, **63**, 32–41.
40. Brünger, A. T., Adams, P. D., Clore, G. M., DeLano, W. L., Gros, P., Grosse-Kunstleve, R. W. *et al.* (1998). Crystallography & NMR system: a new software suite for macromolecular structure determination. *Acta Crystallogr. Sect. D*, **54**, 905–921.
41. Adams, P. D., Afonine, P. V., Bunkoczi, G., Chen, V. B., Davis, I. W., Echols, N. *et al.* (2010). PHENIX: a comprehensive Python-based system for macromolecular structure solution. *Acta Crystallogr. Sect. D*, **66**, 213–221.
42. Murshudov, G. N., Vagin, A. A. & Dodson, E. J. (1997). Refinement of macromolecular structures by the maximum-likelihood method. *Acta Crystallogr. Sect. D*, **53**, 240–255.
43. Skubak, P., Murshudov, G. N. & Pannu, N. S. (2004). Direct incorporation of experimental phase information in model refinement. *Acta Crystallogr. Sect. F*, **60**, 2196–2201.
44. Emsley, P. & Cowtan, K. (2004). Coot: model-building tools for molecular graphics. *Acta Crystallogr. Sect. D*, **60**, 2126–2132.